

4

SECURITY

AD-A197 744

DTIC FILE COPY

RT DOCUMENTATION PAGE

1a. REPORT SECURITY CLASSIFICATION UNCLASSIFIED			1b. RESTRICTIVE MARKINGS		
2a. SECURITY CLASSIFICATION AUTHORITY			3. DISTRIBUTION / AVAILABILITY OF REPORT Approved for public release and sale. Distribution unlimited.		
2b. DECLASSIFICATION / DOWNGRADING SCHEDULE			5. MONITORING ORGANIZATION REPORT NUMBER(S) DTIC SELECTED JUL 27 1988 H		
4. PERFORMING ORGANIZATION REPORT NUMBER(S) ONR Technical Report 19					
6a. NAME OF PERFORMING ORGANIZATION Department of Chemistry	6b. OFFICE SYMBOL (if applicable)	7a. NAME OF MONITORING ORGANIZATION			
6c. ADDRESS (City, State, and ZIP Code) State University of New York at Buffalo Buffalo, New York 14214		7b. ADDRESS (City, State, and ZIP Code)			
8a. NAME OF FUNDING / SPONSORING ORGANIZATION Office of Naval Research	8b. OFFICE SYMBOL (if applicable) ONR	9. PROCUREMENT INSTRUMENT IDENTIFICATION NUMBER N00014-84-K-0052			
8c. ADDRESS (City, State, and ZIP Code) Chemistry Program Arlington, Virginia 22217		10. SOURCE OF FUNDING NUMBERS			
		PROGRAM ELEMENT NO	PROJECT NO	TASK NO NR-051-855	WORK UNIT ACCESSION NO
11. TITLE (Include Security Classification) Corrosion Measurements using Microelectrodes					
12. PERSONAL AUTHOR(S) Kazimierz Wikiel and Janet Ostervang					
13a. TYPE OF REPORT Technical	13b. TIME COVERED FROM TO	14. DATE OF REPORT (Year, Month, Day) 1988 July 8		15. PAGE COUNT	
16. SUPPLEMENTARY NOTATION					
17. COSATI CODES			18. SUBJECT TERMS (Continue on reverse if necessary and identify by block number)		
FIELD	GROUP	SUB-GROUP	corrosion, microelectrodes, ohmic drop		
19. ABSTRACT (Continue on reverse if necessary and identify by block number) It is shown that microelectrodes can be substituted for large area electrodes in typical corrosion measurements. Results obtained for copper and iron in concentrated solutions are consistent with earlier literature reports. Application of microelectrodes markedly reduces effects of IR-ohmic drops. It allows one to apply electrochemical methods in corrosion investigations under conditions closer to those of natural corrosion environments. The corrosion rate of circular copper microelectrodes in 0.1 mol/dm ³ HCl solution depends on radius and increases with decreasing radius.					
20. DISTRIBUTION / AVAILABILITY OF ABSTRACT <input type="checkbox"/> UNCLASSIFIED/UNLIMITED <input checked="" type="checkbox"/> SAME AS RPT <input type="checkbox"/> DTIC USERS			21. ABSTRACT SECURITY CLASSIFICATION UNCLASSIFIED		
22a. NAME OF RESPONSIBLE INDIVIDUAL			22b. TELEPHONE (Include Area Code)		22c. OFFICE SYMBOL

OFFICE OF NAVAL RESEARCH

Contract N00014-84-K-0052

Task No. NR 051-855

TECHNICAL REPORT NO. 19

Corrosion Measurements using Microelectrodes

by

Kazimierz Wikiel and Janet Osteryoung

Published in

Journal of Electrochemical Society

State University of New York at Buffalo
Department of Chemistry
Buffalo, New York 14214

July 1988

Reproduction in whole or in part is permitted for
any purpose of the United States Government.

This document has been approved for public release
and sale; its distribution is unlimited.

Corrosion Measurements Using Microelectrodes

Kazimierz Wikiel¹ and Janet Osteryoung

Department of Chemistry

State University of New York at Buffalo


Buffalo, New York 14214 (USA)

¹Permanent Address: Institute of Precision Mechanics,
00-967 Warsaw, Duchnicka 3, Poland

SUMMARY

It is shown that microelectrodes can be substituted for large area electrodes in typical corrosion measurements. Results obtained for copper and iron in concentrated solutions are consistent with earlier literature reports. Application of microelectrodes markedly reduces effects of IR-ohmic drops. It allows one to apply electrochemical methods in corrosion investigations under conditions closer to those of natural corrosion environments. The corrosion rate of circular copper microelectrodes in 0.1 mol dm⁻³ HCl solution depends on radius and increases with decreasing radius.



Accession For	
NTIS GRA&I	<input checked="" type="checkbox"/>
DTIC TAB	<input type="checkbox"/>
Unannounced	<input type="checkbox"/>
Justification	
By	
Distribution/	
Availability Codes	
Dist	Avail and/or Special
A-1	

INTRODUCTION

Unique features of very small, micrometer-size voltammetric electrodes cause the range of their application to be extended continuously. Microelectrodes have been used to solve neurophysiological problems both in vivo and in vitro [1-6]. Arrays of carbon fibers have been used as a voltammetric detector in high-performance liquid chromatography [7], whereas single ultramicroelectrodes have been applied in fast spectroelectrochemistry [8-10]. Microelectrodes have been used in electrochemical investigations in solvent without background electrolyte in order to reduce the effects of ohmic potential drops [11-16] or to extend the accessible potential range [17,18]. Microelectrodes have made it possible to make electrochemical measurements in such novel media as glass solvent eutectics [19] and the gas phase [20]. Micrometer size electrodes have been used in kinetics studies [21-23] and in investigations of nucleation of mercury at a microelectrode surface [22].

In this report we show that microelectrodes can be substituted for large area electrodes in typical corrosion measurements, and that the application of such small electrodes can give some novel advantages. The main advantage is that very high current densities can be achieved at low currents. Thus ohmic polarization can be made negligible even when the specific conductance of the solution is low. A second advantage is that at small electrodes steady state diffusional profiles are achieved at short times. Thus experiments can be carried out quickly. Finally, the dependence of the response on electrode radius, which is analogous to the dependence on rotation rate for a rotating disk, may prove useful in studies of localized corrosion processes such as pitting.

At an embedded circular electrode of radius r the limiting diffusion-controlled steady-state current for a simple charge transfer process is given by $i_s = 4nFD Cr$, where n is the number of electrons transferred, F the value of the Faraday, and D and C are the diffusion coefficient and bulk concentration, respectively, of reactant.

The steady-state current can be described using a diffusion layer model in which the thickness of the diffusion layer is $\delta = \pi r/4$. In contrast with the corresponding rotating disk case, the diffusion layer thickness does not depend on diffusion coefficient.

Here we describe results for two well-studied processes, the dissolution of iron and copper in deaerated chloride solutions.

EXPERIMENTAL SECTION

Preparation of electrodes. To prepare circular copper electrodes, glass-coated 6 μm (M. Fleischmann) and 10 μm -diameter (Cu-99.99%, Goodfellow) copper wires were used. A piece of glass-coated wire approximately 3 cm long was sealed in vacuum into a 2- μL glass micropipette (Drumond Scientific Co.) to confer mechanical stability and create a larger diameter insulating plane around the active electrode surface. This was done by inserting the glass-coated wire through the pipet, sealing one end, applying a vacuum, and then sealing a portion of the region under vacuum. The wire was then cut at this inner sealed position. This procedure prevented the copper from reacting chemically during the sealing process. In order to prepare the electrical connection, the inner glass coating from the copper wire was removed by using hydrofluoric acid. Then electrical connection was made with a silver thermosetting preparation (P-310 Johnson

Matthey Ltd.) and after that this part was covered with thermally shrinkable tubing. The cross section of copper sealed in glass was polished carefully by using a rotating wheel covered with a CarbiMet paper disk with decreasing grit size and subsequently with Microcloth polishing cloth with 1.0, 0.3 and 0.05- μm alumina suspensions (Buehler Ltd.). The quality of the surface was checked optically with 500x magnification (Leitz-Dievert microscope). Only electrodes without any visible defects on the surface were taken for further experiments. Electrodes were repolished lightly before each experiment.

The preparation of circular iron electrodes (10- μm diameter, glass coated, 99.99% Fe, Goodfellow) was carried out in a similar way. The initial seal between the glass-coated wire and the capillary was made with epoxy, because it was not possible to seal glass to glass directly in the presence of the reactive iron wire. In this case the inner glass coating was removed in molten sodium hydroxide. The resistance of electrodes was about 30, 10 and 70 Ω for 6- μm Cu, 10- μm Cu and 10- μm Fe, respectively, and less than 1 Ω for electrodes with larger radii.

Instrumentation and chemicals. All experimental control, data collection and calculations were carried out on a DEC PDP 8/e laboratory minicomputer interfaced to an EG&G PARC model 273 potentiostat equipped with a Keithley model 427 current amplifier. The reference electrode was saturated calomel and all potentials are quoted with respect to this. A platinum counter electrode was used.

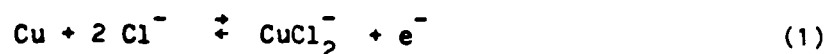
All reagents were of analytical grade, and distilled water passed through a Millipore Milli-Q purification system was used for preparation of the solutions. Solutions were purged with purified argon for at least 20 min. before each experiment. After purging, the argon was directed over the solution.

After a step-wise change in potential the steady-state value of current at an embedded circular electrode is achieved within 5% by time(s) $6 \times 10^6 r^2$, where r is in cm (assuming $D = 9 \times 10^{-6} \text{ cm}^2/\text{s}$). In this work electrodes of $r=3, 5, 12.5$, and 63.5×10^{-4} cm were used. The corresponding times are 0.5, 1.4, 8.9, and 242 s, respectively. Experiments described here were carried out employing a staircase potential-time waveform with 2 mV step height and 2 s period. Thus all the data at the 6 and 10 μm -diameter electrodes are obtained under diffusional steady state conditions, whereas for the 25- μm electrode the first few points should exceed the steady state values. The very long times required to achieve steady-state diffusion at the 127- μm electrode produce a different situation in which relaxation of concentration gradients is promoted by natural convection.

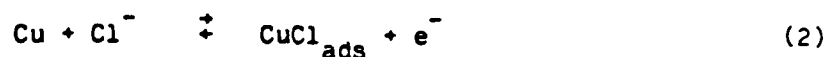
RESULTS AND DISCUSSION

Typical anodic and cathodic polarization curves for a 25- μm diameter copper electrode in deoxygenated $0.1 \text{ mol dm}^{-3} \text{ HCl}$ solution are shown in Fig. 1. The cathodic Tafel plot has a slope of 120 mV/decade which is close to the values reported in the literature [24,25]. The anodic polarization curve consists of two regions and also agrees well with previous reports [25-30]. The first part is a straight line with slope about 60 mV/decade. The second part, occurring at potentials more positive than 0.0 V, has a higher slope. These two regions are separated by a region which displays some oscillations in the current.

The first part corresponds to the diffusion-controlled dissolution of Cu with the formation of CuCl_2^- as a final product, according to the overall equation:



According to Moreau [29,30] this reaction consists of three successive steps:



In this potential region the rate is governed entirely by diffusion on a uniform reaction surface. Braun and Nobe [28] have shown that diffusion of the chloride ions to the electrode surface is the rate-determining step under these conditions. For reaction (1) the Nernstian relation is

$$E = E_{1/2} - (1/f) \ln \{ 2(1 - i/i_d)^2 / (i/i_d) \}$$

$$E_{1/2} = E^\circ_{\text{Cu}^+/\text{Cu}} - (1/f) \ln \{ \beta_2 D_{\text{CuCl}_2} C_{\text{Cl}}^2 / 2 D_{\text{Cl}} \} \quad (5)$$

where $i_d = 4FD_{\text{Cl}}C_{\text{Cl}}r$, $f = F/RT$, and β_2 is the overall formation constant for CuCl_2^- . For small values of i/i_d the quantity $(1 - i/i_d)^2$ may be approximated by unity. In fact the limiting current is not accessible experimentally, so in practice eq. (5) can only be applied when i/i_d is small. Rearranging we obtain

$$i = 4FD_{\text{CuCl}_2} C_{\text{Cl}}^2 \beta_2 r \exp \{ f(E - E^\circ_{\text{Cu}^+/\text{Cu}}) \} \quad (6)$$

Expressing this relation in terms of current density and steady-state diffusion layer thickness, δ_s , we obtain

$$i/A = (FD_{\text{CuCl}_2} C_{\text{Cl}}^2 \beta_2 / \delta_s) \exp \{ f(E - E^\circ_{\text{Cu}^+/\text{Cu}}) \} \quad (7)$$

This expression is equivalent to that derived from the kinetic viewpoint by Smyrl [25]. In Figure 1, the maximum value of i/i_d is about 0.2, so eqn. (7) is a reasonable approximation which predicts the observed slope $\partial \log i / \partial E = 60$ mV. We will return below to the question of dependence on concentration of chloride.

The steady-state voltammogram of Figure 2 shows more clearly the region of current oscillation. The details of the response here vary from experiment to experiment, but the general features are reproducible. Returning to Figure 1, the second part of the anodic copper dissolution curve, occurring beyond the region of current oscillations at more positive potentials, corresponds to transpassive dissolution of copper. Moreau [30], using X-ray diffraction methods, has identified two solid products at the copper surface, CuCl and $\text{Cu}_2(\text{OH})_3\text{Cl}$. Also Cooper and Bartlett [31] have observed formation of Cu(II) during anodic dissolution in this potential region. Up to 30% of the anodic current was attributed to formation of Cu(II) . Overshoots and oscillations at the beginning of this region (cf. Figure 2) were attributed to the formation and dissolution of a multilayer film on the electrode surface [31].

From the above it follows that results obtained at the circular copper microelectrode are in good agreement with the earlier data in the literature. Thus electrodes of small size are certainly appropriate for corrosion measurements. The small size also permits rapid measurements in the steady-state diffusional regime and thus reduces the amount of change in the surface during the course of the measurement. In the present case (Figure 1) with an effective potential scan rate of 1 mV/s, the amount of material lost in scanning from the corrosion potential to the passivation potential corresponds to about 0.3 μm thickness of copper. Halving the scan rate would double that thickness.

The most important feature of the microelectrode is that the same valuable data available from large electrodes can be obtained by measuring very small total currents. At microelectrodes small currents give rise to relatively high current densities. This is shown in Figure 3, which

presents a Tafel plot for anodic dissolution of a smaller (10- μm diameter) circular iron electrode in 1 mol dm^{-3} potassium chloride solution. Usually, even at such high concentrations of supporting electrolyte, anomalies in current-potential plots are observed very easily when conventional-size electrodes are used. These deviations are caused by ohmic iR -drops in the region of higher current densities, even if a Luggin probe is employed. In order to obtain plots of the proper shape, such techniques as positive feedback, current interruption, or some methods of calculations have to be used. This is unnecessary when microelectrodes with very small surface area are used instead of a conventional size electrode. For the microelectrode (Figure 3) a straight line log plot for anodic iron dissolution without any evidence of iR ohmic drops is observed up to 0.2 A/cm^2 , i.e. to the region where some effects connected to the transpassive dissolution of iron have been observed. Moreover a Luggin probe was not used in these experiments.

The anodic Tafel slope for electrodisolution of iron is about 70 mV/decade, close to the value of 80 mV/decade obtained by Asakura and Nobe [32] for the steady-state anodic polarization of iron in the same unbuffered neutral 1 mol dm^{-3} KCl solution. However, their log plot was obtained by using the current interruption method. The apparent potential-log current relation deviated markedly from linearity for current densities above 10 mA/cm^2 .

Obviously, it is almost impossible to obtain a properly shaped potential-current relation at electrodes of "normal" size in solutions with markedly lower conductivity, even if sophisticated methods of ohmic iR -drop correction would be used. For instance, modern instrumentation such as the PARC 273 potentiostat allows one to compensate ohmic iR drops up to 200 Ω at the 10 mA range or up to 2 M Ω at the 1 μA range by using positive feedback.

Since the currents at microelectrodes reach the microampere level only in extreme conditions, ohmic iR drops due to high resistance can be corrected as needed. But this iR compensation is inadequate for even routine conditions at a large electrode.

Anodic dissolution curves for iron in 10^{-4} mol dm^{-3} KCl solution are shown in Fig. 4. Resistivity of this solution is about $60 \text{ k}\Omega \text{ cm}^{-1}$. Curve A, obtained with a $10 \text{ }\mu\text{m}$ -diameter circular electrode, is a straight line up to 10 mA/cm^2 . Small deviations from linearity are observed above this limit. Curve B was obtained with a still small but markedly larger $127\text{-}\mu\text{m}$ diameter iron electrode. No straight line region of the log plot can be identified in this case although the total currents are markedly lower than (less than one-thousandth of) those at electrodes used in typical corrosion measurements. (Note that the maximum current densities are no greater than about 1% of those expected for an anodic reaction diffusion-controlled in chloride.)

Since the use of microelectrodes reduces markedly ohmic iR -drops, it allows one to extend the range of corrosion measurements. As an example of such possibilities the anodic dissolution of copper over a wide range of chloride ions concentrations was chosen.

Anodic polarization curves of copper in chloride ion solutions with various concentration are shown in Fig. 5. A circular electrode with diameter of $6 \text{ }\mu\text{m}$ was used. Concentrations of chloride ions are in the range $1\text{-}10^{-4}$ mol dm^{-3} , and no other electrolytes were added to the solutions. Anodic behavior of copper depends markedly on concentration of chloride ion and can be divided into two regions. Above a concentration of 0.01 mol dm^{-3} log plots of anodic dissolution are straight lines and their slopes are approximately 60 mV/decade . According to Smyrl [25] for rotating disk

steady-state currents the anodic dissolution current density in this region can be described by:

$$1/A = (Fk_a D_{CuCl_2}^{1/2} C_{Cl}^2 / k_c \delta_L) \exp[(\alpha_a + \alpha_c)f(E-E^0)] \quad (8)$$

where k_a and α_a are the anodic rate constant and charge transfer coefficient, respectively, and k_c and α_c are the corresponding cathodic values. The quantity δ_L is the Levich diffusion-layer thickness. The choice of reference potential makes $k_a = k_c$. Other symbols have their usual meanings. Assuming $\alpha_a = \alpha_c = 0.5$ eq. (8) is equivalent to eq. (5) and the slope of a plot of E vs. $\log i$ should be 60 mV/decade. From eq. (8) it follows that current density depends markedly on the concentration of chloride ions. Moreau [29] has investigated the effect of chloride ion concentration on anodic dissolution of copper within the range 0.1 to 10 mol dm^{-3} . He found the value of $(dE/d \log C_{Cl})_{1,298} = 118$ mV. Our results obtained at copper microelectrodes are in good agreement with the theoretical prediction and with earlier reports. The log plot slopes of 60 mV/decade as well as the shift of the anodic curve 120 mV/decade C_{Cl} toward more positive potentials with decreasing chloride concentration down to 0.01 mol dm^{-3} are congruent with literature reports about anodic behavior of copper in solutions with higher chloride concentrations [28-30]. This means that even at chloride concentrations as low as 0.01 mol dm^{-3} the final product of anodic dissolution of copper is $CuCl_2^-$, and that diffusion is rate determining. Generally, in this region of chloride concentration the anodic dissolution of copper is governed by diffusion phenomena on a uniformly active surface.

At very low chloride ion concentration changes in shape of the current-potential curve are observed (Fig. 5, curves D,E). The slope of the log plots is 30-40 mV/decade at about 0.1 mA/cm^2 . It should be mentioned that

reproducibility of the results obtained with low chloride concentration is markedly poorer than in the higher range. The smaller slope probably reflects the same phenomenon as in the oscillation region in the solution with higher chloride concentration, i.e. the formation of multilayer films on the electrode surface. The second part of these curves indicate that transpassive oxidation of copper is involved in the electrodisolution process. It would be extraordinarily difficult to correct for iR drops under these conditions because the specific conductance of the solution changes markedly in the vicinity of the electrode during the course of the experiment [33].

Braun and Nobe [28] have estimated that in solution with chloride ion concentration lower than approximately 0.05 mol dm^{-3} a considerable amount of copper is dissolved as non-chloride-complexed copper(II) ions. The thermodynamic potential for equal concentrations of Cu^{2+} and Cu^+ at the electrode surface is -0.082 V , and CuCl(s) is thermodynamically stable only at more positive potentials. Taking into account only the species Cu^+ , CuCl_2^- and Cu^{2+} , the predominant species is CuCl_2^- except in 10^{-3} and 10^{-4} M Cl^- . For these lower chloride concentrations Cu^+ predominates except at higher current densities ($> 0.6 \text{ mA/cm}^2$) where Cu^{2+} becomes increasingly important. Our results confirm the change of electrodisolution mechanism. However, also in the low chloride concentration range ($1 \times 10^{-3} - 1 \times 10^{-4} \text{ mol dm}^{-3}$) a considerably smaller but still marked effect of chloride ion concentration on copper electrodisolution is observed.

Equation 5 predicts that the current density for copper dissolution should be inversely proportional to the diffusion layer thickness. The influence of diffusion layer thickness on anodic current density of copper in HCl solutions has been reported [25,28,29]. The thickness of the

diffusion layer has been changed by changing the rotation rate of a rotating disk electrode. Current densities were observed to increase as the rotation rate was increased. However, Braun and Nobe [28] have not observed direct proportionality to the square root of the rotation rate. Smyrl [25] has reported a closer fit to the expected dependence. Minor deviations have been observed at very high rotation rates. On the other side, Moreau [29] has reported a value of $(dE/d \log \omega^{1/2})_{1,298} = -59 \text{ mV}$ which is in excellent agreement with eq. (5).

Since at microelectrodes the steady-state diffusion layer thickness is proportional to the electrode radius, anodic current density should be inversely proportional to the radius of a circular microelectrode. Typical curves of anodic dissolution of copper microdisk electrodes with different radii in 0.1 mol dm^{-3} hydrochloric acid are presented in Fig. 6. At the same potential value the anodic current density for smaller electrodes is larger than for larger ones. Since the cathodic process of hydrogen evolution does not depend on diffusion phenomena, the corrosion current density and corrosion potential obtained by extrapolation of straight parts of log plots to their intersection depend on the radius of the microelectrode. The corrosion current density is increased and corrosion potential is shifted toward more negative potentials with decrease in microelectrode radius.

An expression for the corrosion current can be obtained by equating the anodic current (eq. (8)) with the negative of the cathodic current (cf. Fig. 1). Assuming that all transfer coefficients are 0.5, we obtain

$$i_{\text{corr}} = k_{\text{CH}}^{2/3} (D_{\text{Cl}_2} C_{\text{Cl}_2}^{2/3})^{1/3} \quad (9)$$

where k_{CH} is the rate constant for hydrogen reduction at the corrosion potential. Using the value $i^0 = 10^{-6.7} \text{ A/cm}^2$ for reduction of H^+ on Cu

[24], $k_{CH} = 10^{-11.7}$ cm/s. A plot of experimental corrosion current density vs $r^{-1/3}$ for electrodes of radii 3, 5, and 12.5 μm yielded a straight line with correlation coefficient 0.9998 and slope 9.6×10^{-9} A/cm^{5/3}. The slope predicted by eq. (9) with $D_{Cl} = 10^{-5}$ cm²/s is 3.8×10^{-9} A/cm^{5/3}. Considering uncertainties in the data and in the appropriate value of k_{CH} , this is excellent agreement.

The same approach yields the prediction $\partial V_{corr} / \partial \log r = 40$ mV. A plot of E_{corr} vs $\log r$ was linear (correlation coefficient = 0.9996) with slope 26 mV. Thus the shift in corrosion potential is less than predicted.

A final comment on the use of microelectrodes for studying corrosion processes concerns the role of geometry in the formation of single pits. Beck and Alkire have discussed the role of spherical diffusion in formation of pits [34]. The relation confirmed here between size and corrosion rate for a homogeneous surface demonstrates experimentally the prediction of higher corrosion rates at small sites on a heterogeneous surface. Furthermore, it seems feasible to study small electrodes under conditions where only one pit can form and thus to examine more quantitatively models which describe this process, especially in its early stages.

ACKNOWLEDGMENTS

This work was supported in part by the Office of Naval Research. The 6- μm diameter copper wires were supplied by Martin Fleischmann, University of Southampton, Southampton, England.

REFERENCES

1. L. C. Clark, C. Lyons: *Ala. J. Med. Sic.*, 2(4), (1965), 355.
2. R. N. Adams: *Anal. Chem.*, 48, (1976), 1126A.
3. J. L. Ponchon, R. Cespuglio, F. Gonon, M. Jouvet, J. F. Pujol: *Anal. Chem.*, 51, (1979), 1483.
4. M. A. Dayton, J. C. Brown, K. J. Stutts and R. M. Wightman: *Anal. Chem.*, 52, (1980), 945.
5. M. A. Dayton, A. G. Ewing and R. M. Wightman: *Anal. Chem.*, 52, (1980), 2392.
6. A. G. Ewing, M. A. Dayton and R. M. Wightman: *Anal. Chem.*, 53, (1981), 1942.
7. R. M. Wightman, W. L. Candill, J. O. Howell: *Anal. Chem.*, 54, (1982), 2532.
8. R. S. Robinson and R. L. McCreery: *Anal. Chem.*, 53, (1981), 997.
9. R. S. Robinson, C. W. McCurdy and R. L. McCreery: *Anal. Chem.*, 54, (1982), 2356.
10. R. S. Robinson and R. L. McCreery: *J. Electroanal. Chem.*, 182, (1985), 61.
11. R. Lines and V. D. Parker: *Acta Chem. Scand.*, B31, (1977), 369.
12. J. O. Howell and R. M. Wightman: *J. Phys. Chem.*, 88, (1984), 3915.
13. A. M. Bond, M. Fleischmann and J. Robinson: *J. Electroanal. Chem.*, 168, (1984), 299.
14. A. M. Bond, M. Fleischmann and J. Robinson: *J. Electroanal. Chem.*, 172, (1984), 11.
15. A. M. Bond, P. A. Lay: *J. Electroanal. Chem.*, 199, (1986), 285.

16. M. J. Pena, M. Fleischmann and N. Garrard: J. Electroanal. Chem., 220, (1987), 31.
17. J. Cassidy, S. P. Khoo, S. Pons and M. Fleischmann: J. Phys. Chem., 89, (1985), 3933.
18. T. Dibble, S. Bandyopadhyay, J. Ghoroghchian, J. J. Smith, F. Sarfarazi, M. Fleischmann and S. Pons: J. Phys. Chem., 90, (1986), 5275.
19. A. M. Bond, M. Fleischmann and J. Robinson: J. Electroanal. Chem., 180, (1984), 257.
20. J. Ghoroghchian, F. Safarazi, T. Dibble, J. Cassidy, J. J. Smith, A. Russell, G. Dunmore, M. Fleischmann and S. Pons: Anal. Chem., 58, (1986), 2278.
21. J. O. Howell, R. M. Wightman: Anal. Chem., 56, (1984), 524.
22. B. Schafiker, G. J. Hills: J. Electroanal. Chem., 130, (1981), 81.
23. Z. Galus, J. Golas and J. Osteryoung:
24. J. O'M. Bockris and N. Pentland: Trans Faraday Soc., 48, (1952), 833.
25. W. H. Smyrl: in Comprehensive Treatise of Electrochemistry, Vol. 4; p. 97-149, (eds. J.O'M. Bockris, B. E. Conway, E. Yeager, R. E. White), Plenum Press, NY 1981.
26. B. Miller and M. J. Bellavance; J. Electrochem. Soc., 119, (1972), 1510.
27. A. L. Baccarella and J. C. Griess: J. Electrochem. Soc., 120, (1973), 459.
28. M. Braun and K. Nobe: J. Electrochem. Soc., 126, (1979), 1666.
29. A. Moreau: Electrochim. Acta, 26, (1981), 497.
30. A. Moreau: Electrochim. Acta, 26, (1981), 1609.

31. R. S. Cooper and J. H. Bartlett: J. Electrochem. Soc., 105, (1958), 109.
32. S. Asakura and K. Nobe: J. Electrochem. Soc., 118, (1971), 13.
33. M. G. Athayde, O. R. Mattos, and L. Sathler, Electrochim. Acta, 32, (1987), 909-913.
34. T. R. Beck and R. C. Alkire: J. Electrochem. Soc., 126, (1979), 1662-1666.

FIGURE LEGENDS

Figure 1. Anodic and cathodic polarization of copper in $0.1 \text{ mol dm}^{-3} \text{ HCl}$ solution. Circular copper electrode, diameter $25 \text{ }\mu\text{m}$; staircase voltammetry: $t = 2\text{s}$; $\Delta E_s = 2\text{mV}$.

Figure 2. Anodic staircase voltammogram of copper in $0.1 \text{ mol dm}^{-3} \text{ HCl}$. Circular copper electrode, diameter $10 \text{ }\mu\text{m}$; $t = 2\text{s}$; $\Delta E_s = 2 \text{ mV}$.

Figure 3. Anodic polarization of iron in $1 \text{ mol dm}^{-3} \text{ KCl}$ solution. Iron microdisk, $10 \text{ }\mu\text{m}$ in diameter. Staircase voltammetry: $t = 2\text{s}$; $\Delta E_s = 2\text{mV}$.

Figure 4. Anodic polarization of iron in $1 \times 10^{-4} \text{ mol dm}^{-3} \text{ KCl}$ solution. Iron disk: A- $10 \text{ }\mu\text{m}$; B- $127 \text{ }\mu\text{m}$ in diameter. Staircase voltammetry: $t = 2\text{s}$; $\Delta E_s = 2\text{mV}$.

Figure 5. Anodic polarization of copper in chloride solutions: $1 \times 10^{-4} \text{ mol dm}^{-3} \text{ HCl}$ +: A- 0.9999 ; B- 0.0999 ; C- 0.0099 ; D- 0.0009 ; E- 0.0000 $\text{mol dm}^{-3} \text{ KCl}$. Copper microdisk, $6 \text{ }\mu\text{m}$ in diameter. Staircase voltammetry: $t = 2\text{s}$; $\Delta E_s = 2\text{mV}$.

Figure 6. Anodic polarization of copper in $0.1 \text{ mol dm}^{-3} \text{ HCl}$ solution. Copper microdisk: A- $6 \text{ }\mu\text{m}$; B- $25 \text{ }\mu\text{m}$ in diameter. Staircase voltammetry: $t = 2\text{s}$; $\Delta E_s = 2 \text{ mV}$.

FIGURE 1

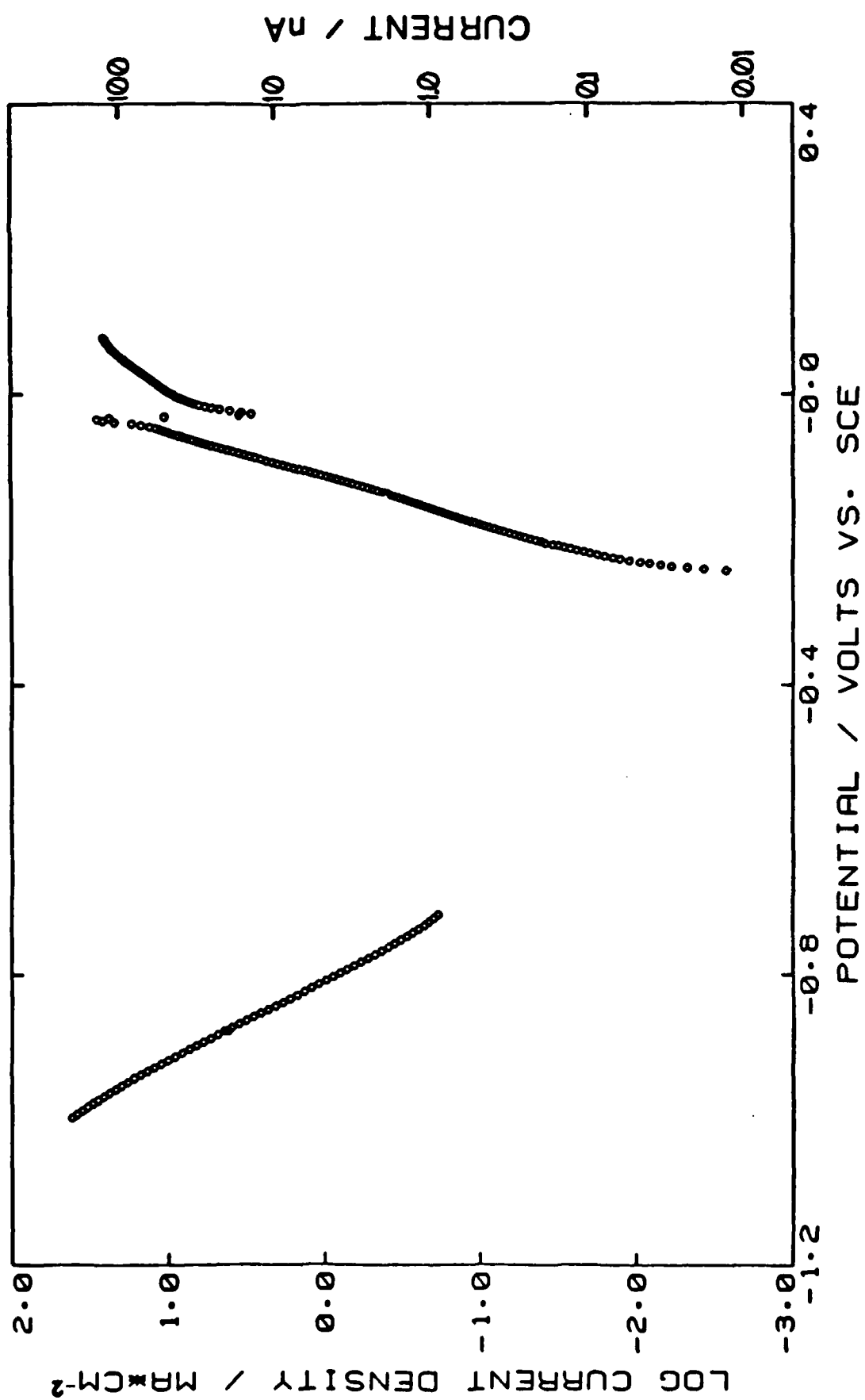


FIGURE 2

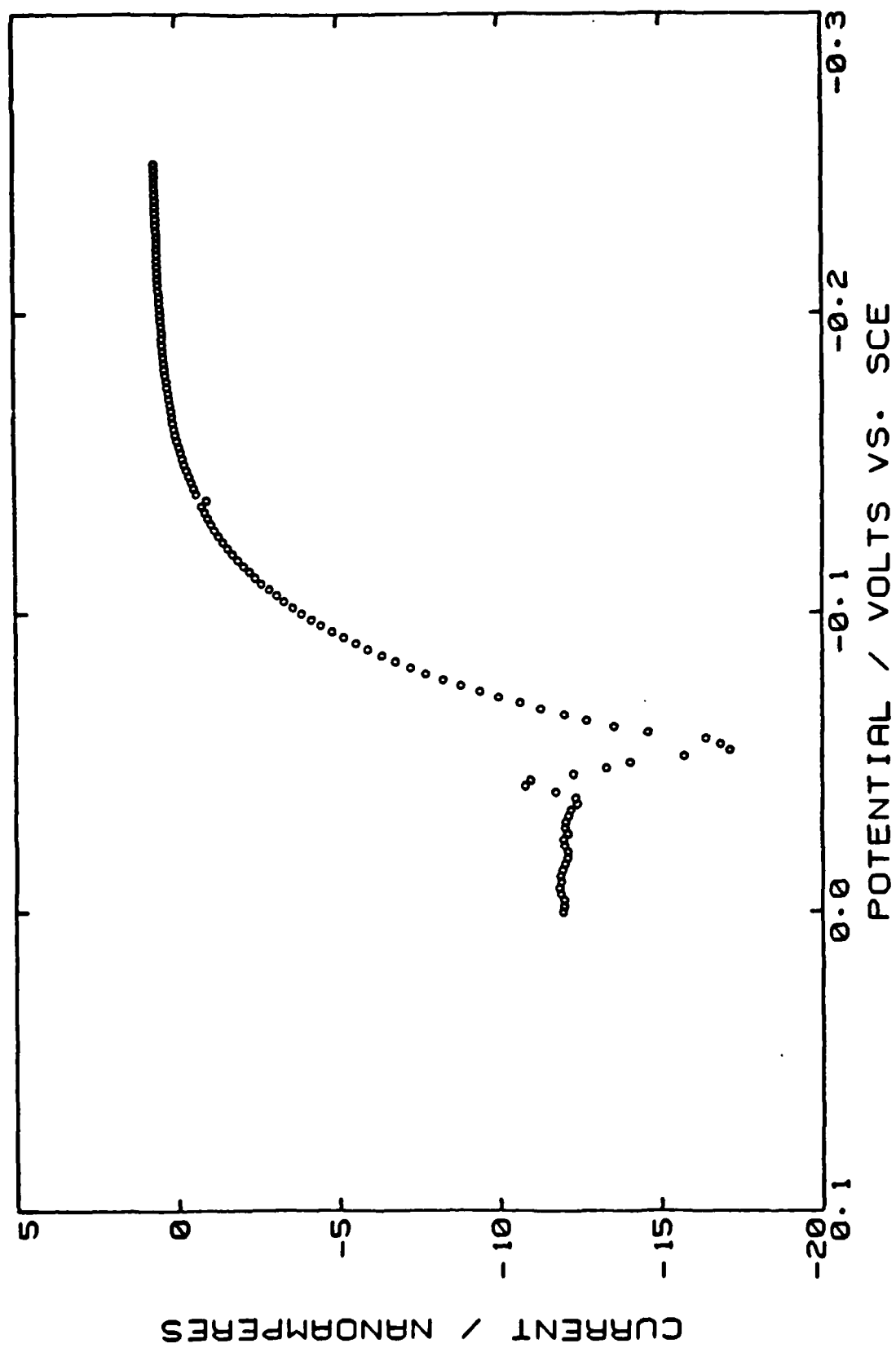


FIGURE 3

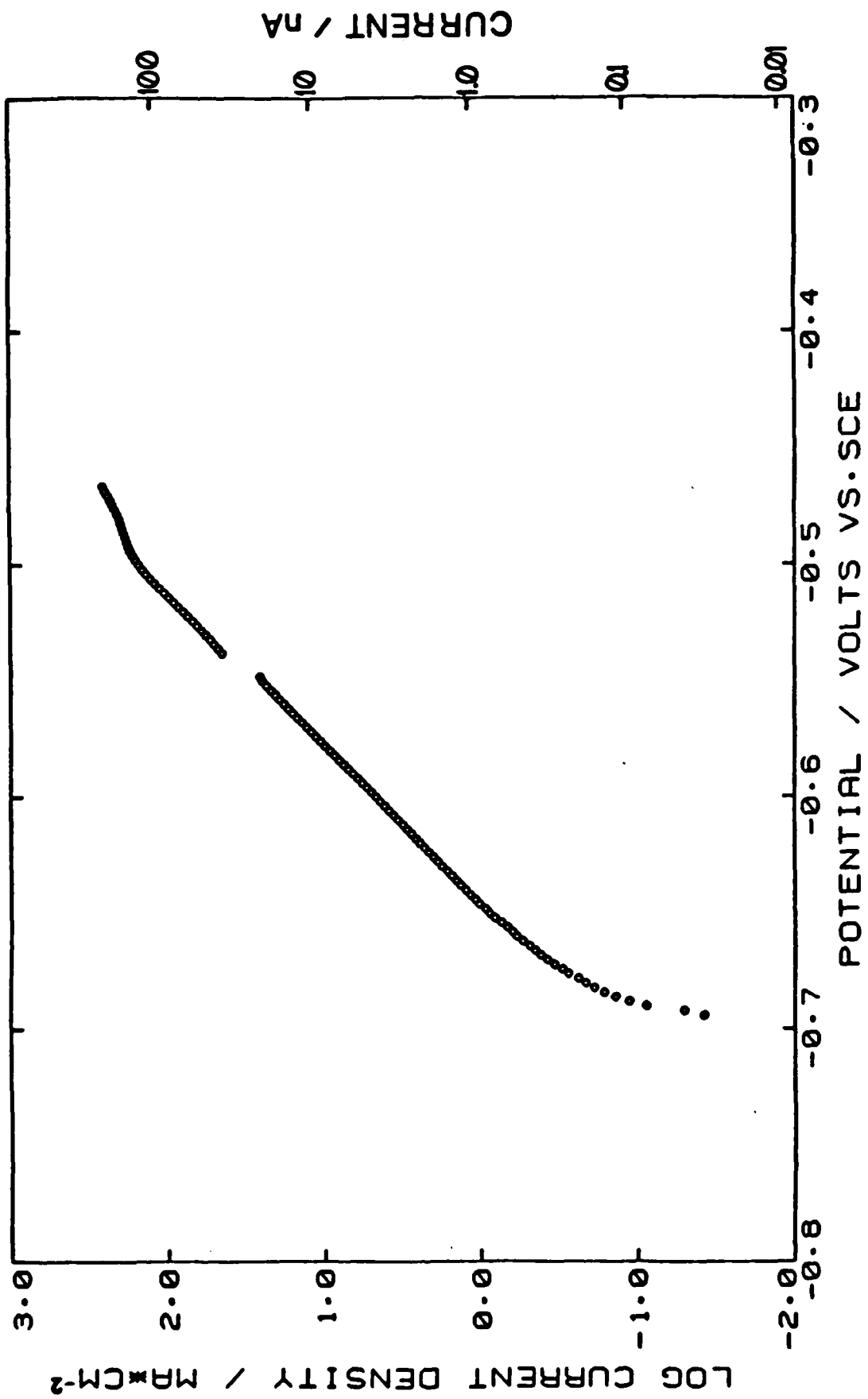


FIGURE 4

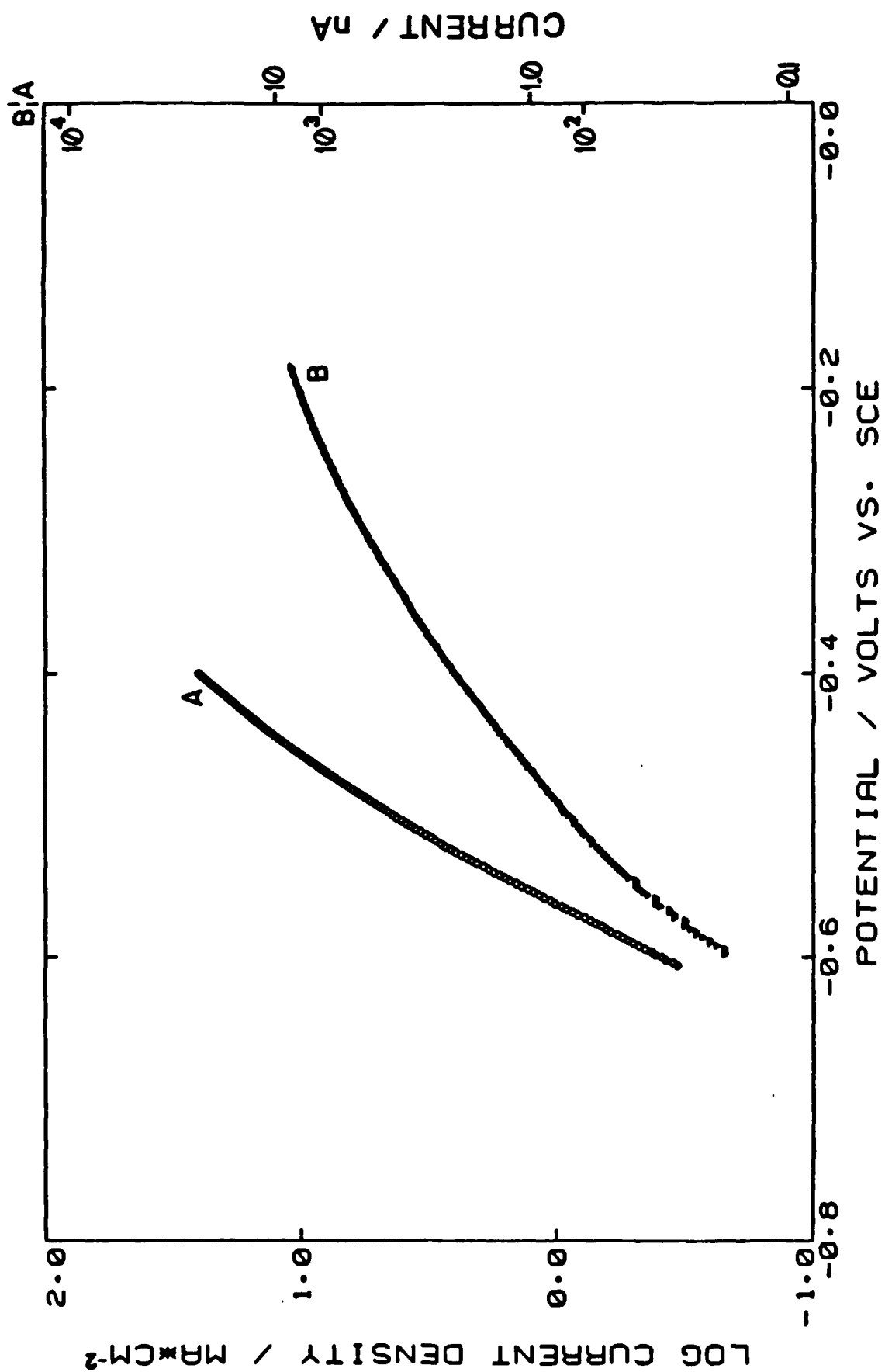


FIGURE 5

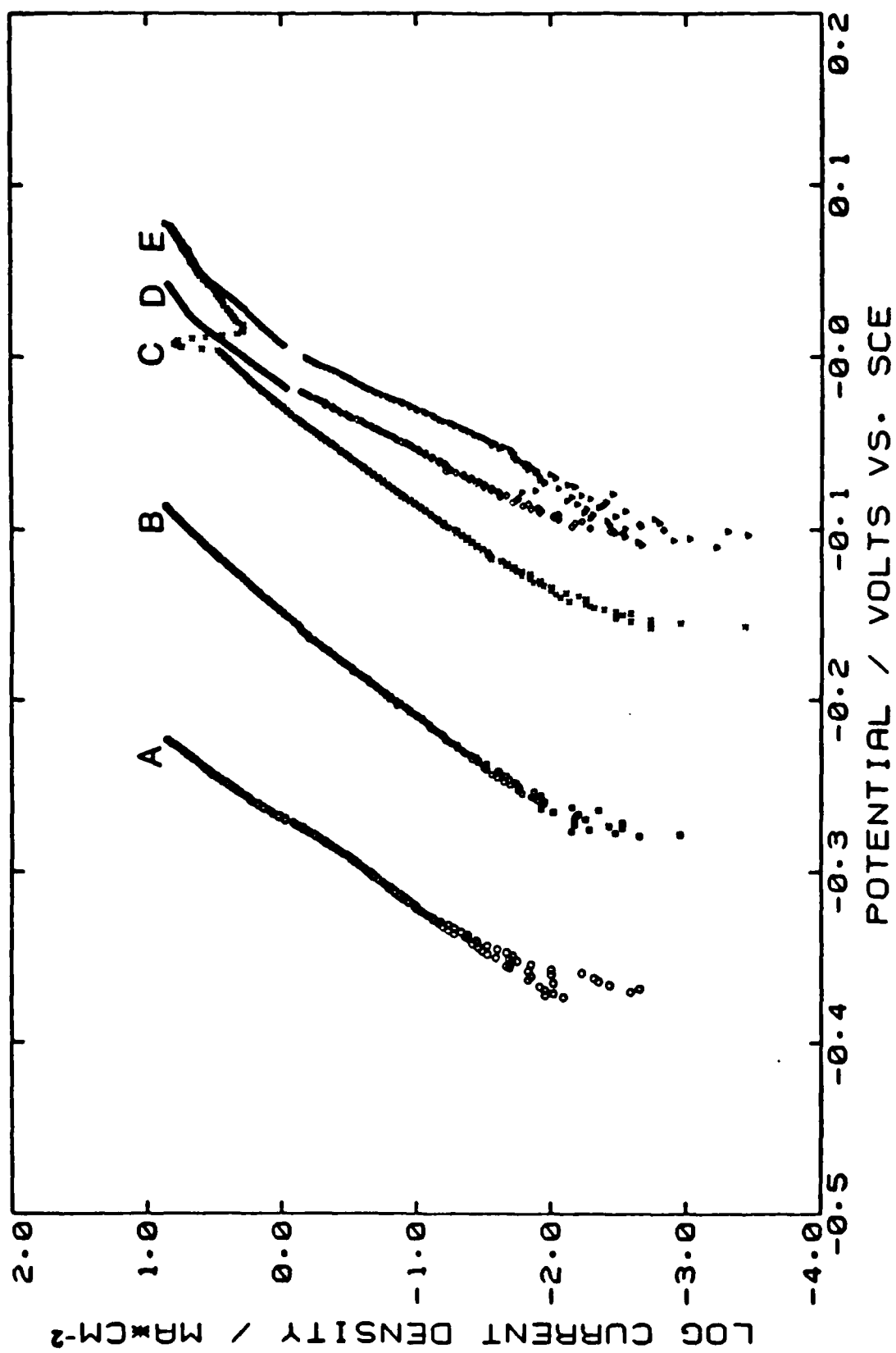
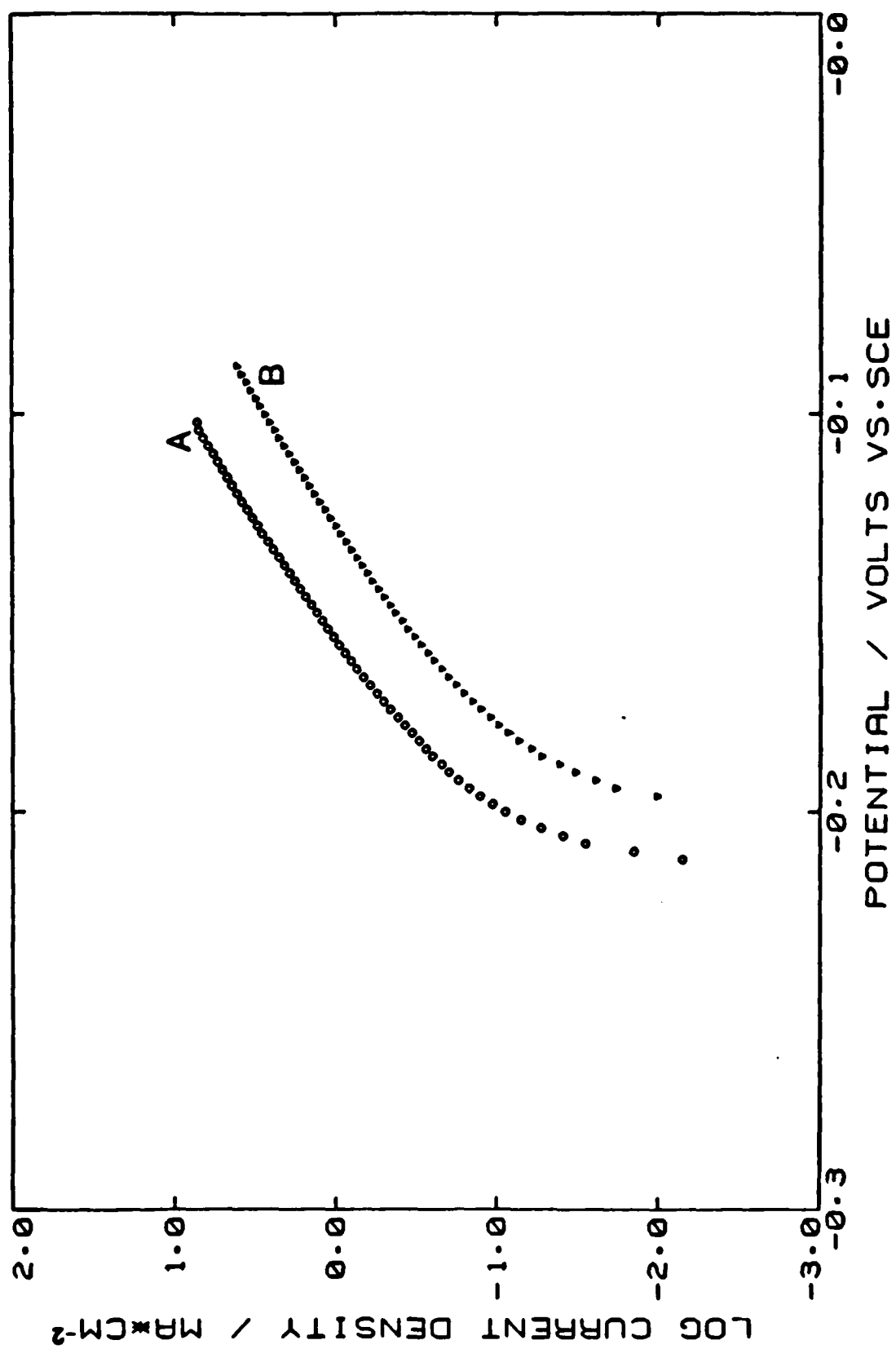


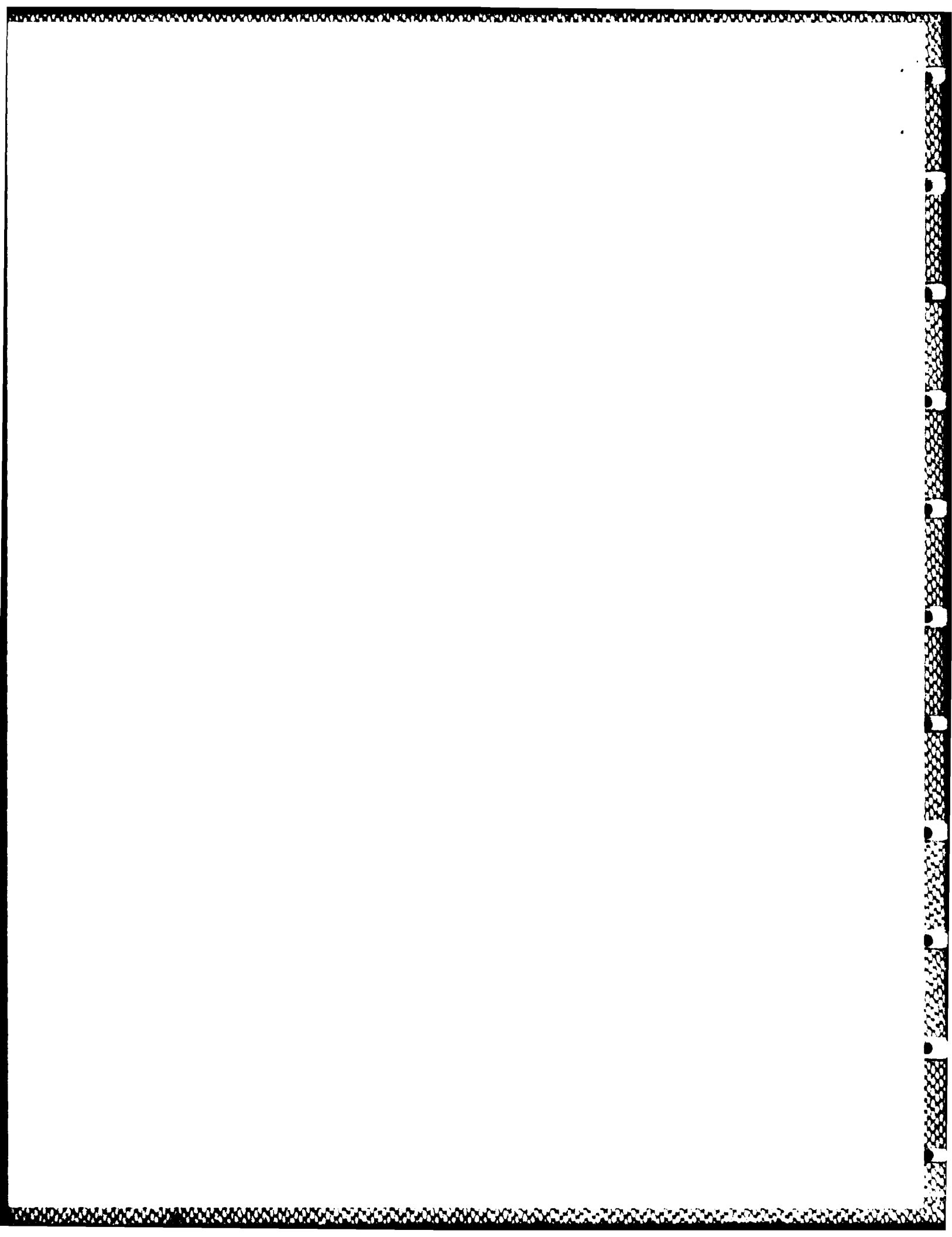
FIGURE 6



DL/1113/87/2

TECHNICAL REPORT DISTRIBUTION LIST, GEN

	<u>No. Copies</u>		<u>No. Copies</u>
✓ Office of Naval Research Attn: Code 1113 800 N. Quincy Street Arlington, Virginia 22217-5000	2	✓ Dr. David Young Code 334 NORDA NSTL, Mississippi 39529	1
✓ Dr. Bernard Douda Naval Weapons Support Center Code 50C Crane, Indiana 47522-5050	1	✓ Naval Weapons Center Attn: Dr. Ron Atkins Chemistry Division China Lake, California 93555	1
✓ Naval Civil Engineering Laboratory Attn: Dr. R. W. Drisko, Code L52 Port Hueneme, California 93401	1	✓ Scientific Advisor Commandant of the Marine Corps Code RD-1 Washington, D.C. 20380	1
✓ Defense Technical Information Center Building 5, Cameron Station Alexandria, Virginia 22314	12 high quality	✓ U.S. Army Research Office Attn: CRD-AA-IP P.O. Box 12211 Research Triangle Park, NC 27709	1
DTNSRDC ✓ Attn: Dr. H. Singerman Applied Chemistry Division Annapolis, Maryland 21401	1	✓ Mr. John Boyle Materials Branch Naval Ship Engineering Center Philadelphia, Pennsylvania 19112	1
✓ Dr. William Tolles Superintendent Chemistry Division, Code 6100 Naval Research Laboratory Washington, D.C. 20375-5000	1	✓ Naval Ocean Systems Center Attn: Dr. S. Yamamoto Marine Sciences Division San Diego, California 91232	1



ABSTRACTS DISTRIBUTION LIST, 359/627

Dr. Stanislaw Szpak
Naval Ocean Systems Center
Code 633, Bayside
San Diego, California 95152

Dr. Gregory Farrington
Department of Materials Science
and Engineering
University of Pennsylvania
Philadelphia, Pennsylvania 19104

Dr. John Fontanella
Department of Physics
U.S. Naval Academy
Annapolis, Maryland 21402-5062

Dr. Micha Tomkiewicz
Department of Physics
Brooklyn College
Brooklyn, New York 11210

Dr. Lesser Blum
Department of Physics
University of Puerto Rico
Rio Piedras, Puerto Rico 00931

Dr. Joseph Gordon, II
IBM Corporation
5600 Cottle Road
San Jose, California 95193

Dr. Joel Harris
Department of Chemistry
University of Utah
Salt Lake City, Utah 84112

Dr. J. O. Thomas
University of Uppsala
Institute of Chemistry
Box 531 Baltimore, Maryland 21218
S-751 21 Uppsala, Sweden

Dr. John Owen
Department of Chemistry and
Applied Chemistry
University of Salford
Salford M5 4WT UNITED KINGDOM

Dr. O. Stafsudd
Department of Electrical Engineering
University of California
Los Angeles, California 90024

Dr. Boone Owens
Department of Chemical Engineering
and Materials Science
University of Minnesota
Minneapolis, Minnesota 55455

Dr. Johann A. Joebstl
USA Mobility Equipment R&D Command
DRDME-EC
Fort Belvoir, Virginia 22060

Dr. Albert R. Landgrebe
U.S. Department of Energy
M.S. 6B025 Forrestal Building
Washington, D.C. 20595

Dr. J. J. Brophy
Department of Physics
University of Utah
Salt Lake City, Utah 84112

Dr. Charles Martin
Department of Chemistry
Texas A&M University
College Station, Texas 77843

Dr. Milos Novotny
Department of Chemistry
Indiana University
Bloomington, Indiana 47405

Dr. Mark A. McHugh
Department of Chemical Engineering
The Johns Hopkins University
Baltimore, Maryland 21218

Dr. D. E. Irish
Department of Chemistry
University of Waterloo
Waterloo, Ontario, Canada
N2L 3G1

DL/1113/87/2

ABSTRACTS DISTRIBUTION LIST, 0518

Dr. R. A. Osteryoung
Department of Chemistry
State University of New York
Buffalo, New York 14214

~~Dr. J. Osteryoung~~
~~Department of Chemistry~~
~~State University of New York~~
~~Buffalo, New York 14214~~

Dr. B. R. Kowalski
Department of Chemistry
University of Washington
Seattle, Washington 98105

Dr. A. Zirino
Naval Undersea Center
San Diego, California 92132

Dr. George H. Morrison
Department of Chemistry
Cornell University
Ithaca, New York 14853

Dr. S. P. Perone
Lawrence Livermore National
Laboratory L-370
P.O. Box 808
Livermore, California 94550

Dr. M. B. Denton
Department of Chemistry
University of Arizona
Tucson, Arizona 85721

Dr. M. Robertson
Electrochemical Power Sources Division
Code 305
Naval Weapons Support Center
Crane, Indiana 47522

Dr. G. M. Kieftje
Department of Chemistry
Indiana University
Bloomington, Indiana 47401

Dr. Christie G. Enke
Department of Chemistry
Michigan State University
East Lansing, Michigan 48824

Walter G. Cox, Code 3632
Naval Underwater Systems Center
Building 148
Newport, Rhode Island 02840

Professor Isiah M. Warner
Department of Chemistry
Emory University
Atlanta, Georgia 30322

Dr. Kent Eisentraut
Air Force Materials Laboratory
Wright-Patterson AFB, Ohio 45433

Dr. John Eyler
Department of Chemistry
University of Florida
Gainesville, Florida 32611

Dr. B. E. Douda
Chemical Sciences Branch
Code 50 C
Naval Weapons Support Center
Crane, Indiana 47322

Professor J. Janata
Department of Bioengineering
University of Utah
Salt Lake City, Utah 84112

Dr. J. DeCorpo
NAVSEA
Code 05 R32
Washington, D.C. 20362

Dr. Ron Flemming
B 108 Reactor
National Bureau of Standards
Washington, D.C. 20234

Dr. Frank Herr
Office of Naval Research
Code 422CB
800 N. Quincy Street
Arlington, Virginia 22217

Dr. Marvin Wilkerson
Naval Weapons Support Center
Code 30511
Crane, Indiana 47522

ABSTRACTS DISTRIBUTION LIST, 359/627

Dr. Manfred Breiter
Institut für Technische Elektrochemie
Technischen Universität Wien
9 Getreidemarkt, 1160 Wien
AUSTRIA

Dr. E. Yeager
Department of Chemistry
Case Western Reserve University
Cleveland, Ohio 44106

Dr. R. Sutula
The Electrochemistry Branch
Naval Surface Weapons Center
Silver Spring, Maryland 20910

Dr. R. A. Marcus
Department of Chemistry
California Institute of Technology
Pasadena, California 91125

Dr. J. J. Auborn
AT&T Bell Laboratories
600 Mountain Avenue
Murray Hill, New Jersey 07974

Dr. M. S. Wrighton
Chemistry Department
Massachusetts Institute
of Technology
Cambridge, Massachusetts 02139

Dr. B. Stanley Pons
Department of Chemistry
University of Utah
Salt Lake City, Utah 84112

Dr. Bernard Spielvogel
U.S. Army Research Office
P.O. Box 12211
Research Triangle Park, NC 27709

Dr. Mel Miles
Code 3852
Naval Weapons Center
China Lake, California 93555

Dr. P. P. Schmidt
Department of Chemistry
Oakland University
Rochester, Michigan 48063

Dr. Roger Belt
Litton Industries Inc.
Airtron Division
Morris Plains, NJ 07950

Dr. Ulrich Stimming
Department of Chemical Engineering
Columbia University
New York, NY 10027

Dr. Royce W. Murray
Department of Chemistry
University of North Carolina
Chapel Hill, North Carolina 27514

Dr. Michael J. Weaver
Department of Chemistry
Purdue University
West Lafayette, Indiana 47907

Dr. R. David Rauh
EIC Laboratories, Inc.
Norwood, Massachusetts 02062

Dr. Edward M. Eyring
Department of Chemistry
University of Utah
Salt Lake City, UT 84112

Dr. M. M. Nicholson
Electronics Research Center
Rockwell International
3370 Miraloma Avenue
Anaheim, California

Dr. Nathan Lewis
Department of Chemistry
Stanford University
Stanford, California 94305

Dr. Hector D. Abruna
Department of Chemistry
Cornell University
Ithaca, New York 14853

Dr. A. B. P. Lever
Chemistry Department
York University
Downsview, Ontario M3J 1P3

ABSTRACTS DISTRIBUTION LIST, 051B

DL/1113/87/2

Dr. Alice Harper
Code 3851
Naval Weapons Center
China Lake, California 93555

Dr. J. Wyatt
Naval Research Laboratory
Code 6110
Washington, D.C. 20375-5000

Dr. J. MacDonald
Code 6110
Naval Research Laboratory
Washington, D.C. 20375-5000

Dr. Andrew T. Zander P1207
Perkin-Elmer Corporation
901 Ethan Allen Highway/MS905
Ridgefield, Connecticut 06877

Dr. A. B. Ellis
Department of Chemistry
University of Wisconsin
Madison, Wisconsin 53706

Dr. Robert W. Shaw
U.S. Army Research Office
Box 12211
Research Triangle Park, NC 27709

Dr. John Hoffsommer
Naval Surface Weapons Center
Building 30 Room 208
Silver Spring, Maryland 20910

ABSTRACTS DISTRIBUTION LIST, 359/627

Dr. Martin Fleischmann
Department of Chemistry
University of Southampton
Southampton SO9 5H UNITED KINGDOM

Dr. John Wilkes
Department of the Air Force
United States Air Force Academy
Colorado Springs, Colorado 80840-6528

Dr. R. A. Osteryoung
Department of Chemistry
State University of New York
Buffalo, New York 14214

Dr. Janet Osteryoung
Department of Chemistry
State University of New York
Buffalo, New York 14214

Dr. A. J. Bard
Department of Chemistry
University of Texas
Austin, Texas 78712

Dr. Steven Greenbaum
Department of Physics and Astronomy
Hunter College
695 Park Avenue
New York, New York 10021

Dr. Donald Sandstrom
Boeing Aerospace Co.
P.O. Box 3999
Seattle, Washington 98124

Mr. James R. Moden
Naval Underwater Systems Center
Code 3632
Newport, Rhode Island 02840

Dr. D. Rolison
Naval Research Laboratory
Code 6171
Washington, D.C. 20375-5000

Dr. D. F. Shriver
Department of Chemistry
Northwestern University
Evanston, Illinois 60201

Dr. Alan Bewick
Department of Chemistry
The University of Southampton
Southampton, SO9 5NH UNITED KINGDOM

Dr. Edward Fletcher
Department of Mechanical Engineering
University of Minnesota
Minneapolis, Minnesota 55455

Dr. Bruce Dunn
Department of Engineering &
Applied Science
University of California
Los Angeles, California 90024

Dr. Elton Cairns
Energy & Environment Division
Lawrence Berkeley Laboratory
University of California
Berkeley, California 94720

Dr. Richard Pollard
Department of Chemical Engineering
University of Houston
Houston, Texas 77004

Dr. M. Philpott
IBM Research Division
Mail Stop K 33/801
San Jose, California 95130-6099

Dr. Martha Greenblatt
Department of Chemistry, P.O. Box 939
Rutgers University
Piscataway, New Jersey 08855-0939

Dr. Anthony Sammells
Eltron Research Inc.
4260 Westbrook Drive, Suite 111
Aurora, Illinois 60505

Dr. C. A. Angell
Department of Chemistry
Purdue University
West Lafayette, Indiana 47907

Dr. Thomas Davis
Polymers Division
National Bureau of Standards
Gaithersburg, Maryland 20899

DL/1113/87/2

ABSTRACTS DISTRIBUTION LIST, 359/627

Dr. Henry S. White
Department of Chemical Engineering
and Materials Science
151 Amundson Hall
421 Washington Avenue, S.E.
Minneapolis, Minnesota 55455

Dr. Daniel A. Buttry
Department of Chemistry
University of Wyoming
Laramie, Wyoming 82071

Dr. W. R. Fawcett
Department of Chemistry
University of California
Davis, California 95616

Dr. Peter M. Blonsky
Eveready Battery Company, Inc.
25225 Detroit Road, P.O. Box 45035
Westlake, Ohio 44145